



**HAL**  
open science

## Displacement damage effects in InGaAs photodiodes produced by electrons, protons and neutrons irradiations

Christophe Inguibert, Thierry Nuns, Juan Barbero, Juan Moreno, Samuel Ducret, Alexandru Neldecu, Bjorn Galmander, Elke Passoth

### ► To cite this version:

Christophe Inguibert, Thierry Nuns, Juan Barbero, Juan Moreno, Samuel Ducret, et al.. Displacement damage effects in InGaAs photodiodes produced by electrons, protons and neutrons irradiations. European Conference on Radiation and its Effects on Components and Systems (RADECS) 2019, Sep 2019, Montpellier, France. hal-02798886

**HAL Id: hal-02798886**

**<https://hal.science/hal-02798886>**

Submitted on 5 Jun 2020

**HAL** is a multi-disciplinary open access archive for the deposit and dissemination of scientific research documents, whether they are published or not. The documents may come from teaching and research institutions in France or abroad, or from public or private research centers.

L'archive ouverte pluridisciplinaire **HAL**, est destinée au dépôt et à la diffusion de documents scientifiques de niveau recherche, publiés ou non, émanant des établissements d'enseignement et de recherche français ou étrangers, des laboratoires publics ou privés.

# Displacement damage effects in InGaAs photodiodes produced by electrons, protons and neutrons irradiations

C. Inguibert<sup>1</sup>, T. Nuns<sup>1</sup>, J. Barbero<sup>2</sup>, J. Moreno<sup>2</sup>, S. Ducret<sup>3</sup>, A. Nedelcu<sup>3</sup>, B. Galnander<sup>4</sup>, E. Passoth<sup>4</sup>

**Abstract**— A set of different InGaAs photodiodes coming from different manufacturers has been irradiated with electrons from 0.5 MeV up to 20 MeV, with protons of 60 MeV, 100 MeV and 170 MeV and with an atmospheric-like neutrons spectrum. Depending on the type of incident particles and energy, the deposited damage dose goes from  $\sim 5 \cdot 10^{+06}$  MeV/g up to  $5 \cdot 10^{+09}$  MeV/g. The dark current damage factor has been extracted from measurements made at different fluence levels. The dark current has been measured a short time after irradiation and two months later to evaluate any possible annealing processes. The damage factor measured after  $\sim$ two months has been scaled according to the Non Ionizing Energy Loss (NIEL). The reliability of the NIEL scaling law is discussed for InGaAs material.

**Index Terms**— Space Environment, Displacement Damage, gamma rays, Non Ionizing Energy Loss.

## I. INTRODUCTION

Energetic particles, when they travel through the matter, interact with the atoms' nuclei and displace them, producing defects in monocrystalline lattices. The fluxes of particles encountered in space are big enough to be able to produce a sufficient amount of defects and degrade significantly the semiconductor materials. The produced electrically active defects act as generation/recombination centres affecting the functioning of the electronic devices. Optoelectronic components are particularly sensitive to such kind of phenomenon. Some degradations, like the increase in dark current are proportional to the amount of defects. In this case, the degradation is thus proportional to the incident fluence. However, the capability of the incident particles to produce defects varies from particle to particle, and even for a given particle type, from an energy to another. The damage coefficient is defined as the ratio of dark current increase by the incident fluence. Hence, the damage coefficient differs from a type of radiation to another. It also depends on the incident energy. Therefore, the fluence is not the best metric to

scale the degradation induced by the displacement damage effects. Indeed, the number of produced defect is proportional to the energy dissipated in the target material by the incident particles. The incident particles put into motion the nuclei of the target material thanks to nuclear interactions (Coulombic, elastic and inelastic). According to the binary collision approximation, the number of displaced atoms is demonstrated to be equal to the dissipated energy divided by twice the minimum energy required to displace an atom ( $T_d$ ). To the first order, the final number of defects is shown to be proportional to the number of atomic displacements and thus to the energy dissipated in terms of nuclear interactions, i.e. the Displacement Damage Dose (DDD). The displacement damage dose deposited per incident particle is given by the Non Ionizing Energy Loss (NIEL) [1]-[5], which is shown to be the best parameter to scale the degradations induced in microelectronic devices by atomic displacements. The well-known "NIEL scaling approach", that consists in considering that the damage factor is proportional to the NIEL, is shown to work quite well in most of cases [6]-[9]. Apart from some deviations observed for electrons [10]-[21] in both Si and GaAs, high energy protons in GaAs [22]-[23] and neutrons in GaAs [24], the NIEL scaling approach is proven to be effective for silicon and gallium arsenide material, for which it is widely used [6]-[9].

It is for electrons that the discrepancies with the NIEL are observed most frequently. These deviations are measured whatever the semiconductor: Si [7][16][17][20] and GaAs [10]-[15][18][19][21].

Furthermore, space applications in the infrared domain have been growing rapidly, requiring a good knowledge of the reliability to radiation of some semiconductor materials such as II-VI (HgCdTe), or III-V (InGaAs). Compared to Si and GaAs, the InGaAs material has not been extensively studied. Extracting some general rules requires a large set of measurements obtained with various particles and energies [25]. The data from the literature that can be used to achieve this task, come from different devices having different technological characteristics that can affect the measured damage factor. Often, the damage factors of different electrical parameters (dark current, diffusion length) are mixed. However, the response to radiations can vary from a parameter to another. For example, in solar cells the degradation of the short circuit current differs slightly from the power loss. In addition, from a reference to another, the test

(1) C. Inguibert, T. Nuns are with ONERA, 2 av. E. Belin, 31055 Toulouse, France (e-mail: christophe.inguibert@onera.fr tel: +33-562252734).

(2) J. Barbero, J. Moreno are with ATN ALTER TECHNOLOGY TÜV NORD S.A.U., C/ Majada 3, 28760 Tres Cantos – Madrid, Spain. (e-mail: [juan.barbero@altertechnology.com](mailto:juan.barbero@altertechnology.com) tel: +34-918041893).

(3) S. Ducret, A. Nedelcu are with LYNRED, 364, route de Valence - Actipole - CS 10021 38113. Veurey-Voroize, France.

(4) B. Galnander, E. Passoth are with TSL hunbergsvägen 5A, 751 21 Uppsala, Sweden.

conditions are not identical. The temperature and the annealing time impact directly the measurements.

The aim of this work is to measure the degradation of a given electrical parameter, the dark current, with a single set of devices, tested with identical conditions. The largest possible set of irradiation conditions is applied on this set of devices. It is then possible to analyse the reliability of the NIEL scaling approach for InGaAs material, based on a large set of irradiation measurements.

Three devices coming from three different manufacturers (Excelitas, OSI, LYNRED) have been tested with electrons of 5 different energies (0.5 MeV, 1.5 MeV, 6 MeV, 12 MeV, 20 MeV). They have also been irradiated with protons of 60 MeV, 100 MeV, and 170 MeV and with an atmospheric-like neutron spectrum (equivalent damage energy of  $\sim 2$  MeV). The damage factor has been extracted and compared to the NIEL calculated with the NEMO [4] package of ONERA implemented in the OMERE [30] toolkit. This work has been performed in the frame of the ROVER project funded by the European Defence Agency (EDA) [29].

The section II presents the experimental setup, describing the devices in study, the irradiation facilities, the test and irradiation conditions. The section III presents some results of dark current increase and the section IV discusses the dark current damage factor of the different irradiation conditions with the NIEL scaling.

## II. EXPERIMENTAL SETUP

### A. Tested photodiodes

Three photodiodes coming from three different manufacturers (Excelitas, OSI, Lynred) have been tested during the irradiation campaigns. Lynred [31] provided test vehicles of the SNAKE device which is an array of InGaAs PIN photodiodes that operate in the  $0.9 \mu\text{m}$  to  $1.7 \mu\text{m}$  wavelength domain. The SNAKE device is a new generation of VGA InGaAs FPA sensor with a high level of sensitivity and resolution dedicated to low flux applications. The test vehicles consist in a set of circular single photodiodes of different dimensions (diameter in the range  $[4 \mu\text{m}, 300 \mu\text{m}]$ ) and  $10 \times 10$  sub-arrays of pixels with various pitches (in the range  $[10 \mu\text{m}, 30 \mu\text{m}]$ ) where all pixels are addressed in parallel. A maximum of six different elements, selected within the available topologies of the test vehicles, are measured during this study, but for some irradiation conditions, there are less measured diodes. Because the test vehicles may have some slight differences in terms of available photodiode dimensions, the measured photodiodes may change from sample to sample and, as a consequence, from one irradiation to another. For this reason, the results will mainly focus on the damage factor and the influence of the size of the photodiodes on the degradation. The measurements presented in this paper are performed at  $-5$  V.

The second tested device is the PIN photodiode C30618 from Excelitas [32]. This high speed single InGaAs circular photodiode is designed for use in OEM fiber-optics communications systems and high-speed receiver applications. It operates between  $1000 \text{ nm}$  and  $1600 \text{ nm}$  and has a diameter

of  $350 \mu\text{m}$  and a maximum intrinsic dark current of typical  $\sim 1 \text{ nA}$  with an applied voltage of  $-10\text{V}$  (the bias at which the current measurements were made).

The last tested device is the FCIQ1000 from OSI [33]. The FCI-InGaAs-QXXX series are large active circular area InGaAs photodiodes segmented into four quadrants. As a consequence, each device has four photodiodes that are all measured independently in our study. In the graph results, they are arbitrarily numbered from 1 to 4. The Q1000 device has an active area of  $1000 \mu\text{m}$  diameter and presents a  $0.5 \text{ nA}$  dark current at  $-5\text{V}$  (bias for the current measurements). The Q1000 photodiode is optimized for a good responsivity from  $1100 \text{ nm}$  to  $1620 \text{ nm}$ .

The two latter devices have been selected because they have relatively large active areas of several hundreds of micrometers of diameter, and present relatively low intrinsic dark currents. The goal was to have the optimal conditions in order to get the best sensitivity to radiation. Because all the irradiated samples are the same whatever the irradiation conditions, the data obtained on these devices are used for a direct comparison of the bias, annealing, particle type and energy, bias conditions effects.

### B. Irradiation facilities

The three devices presented in the previous section have been irradiated with protons, electrons, neutrons and gammas thanks to five different facilities. Two electron energies ( $0.5$  and  $1.5 \text{ MeV}$ ) were performed at the GEODUR facility of ONERA (Toulouse, France) [26] associated with a Van de Graaff accelerator providing mono-energetic beams. The fluxes can be selected from  $1 \text{ nA/cm}^2/\text{s}$  up to  $100 \text{ nA/cm}^2/\text{s}$  ( $10^9 - 10^{12} \text{ e-/cm}^2/\text{s}$ ) with an inhomogeneity lower than  $10\%$  within a beam of  $16 \text{ cm}$  diameter.

Three higher electron energies ( $6 \text{ MeV}$ ,  $12 \text{ MeV}$  and  $20 \text{ MeV}$ ) were performed at the RADEF facility (LINAC of the University of Jyväskylä, Finland) [27]. This pulsed electron beam provides average dose rates ranging from  $100 \text{ rad(water)/min}$  in water up to  $10 \text{ Gy(water)/min}$ . The beam inhomogeneity is lower than  $5\%$  over a square of  $20 \text{ cm} \times 20 \text{ cm}$ .

Some devices have also been irradiated with protons of  $60 \text{ MeV}$ ,  $100 \text{ MeV}$ , and  $170 \text{ MeV}$ , as well as with the atmospheric-like neutron spectrum of The Svedberg Laboratory (TSL, Uppsala, Sweden) facility [28]. Protons are produced thanks to the Gustaf Werner cyclotron performing beam intensities from  $10 \mu\text{A}$  down to single protons per second. They are delivered to the PAULA user facility (Proton Facility in Uppsala). The non-uniformity of the beam was  $<10\%$  at the largest beam diameter ( $\sim 20 \text{ cm}$ ). Neutrons are delivered to the Quasi-Monoenergetic Neutron (QMN) facility and the ANITA facility (Atmospheric-like Neutrons from thick Target). The spallation neutrons of the ANITA spectrum are created in a tungsten target. The neutron beams have a continuous spectrum (Fig. 1) going from thermal energies up to  $\sim 180 \text{ MeV}$ . The neutron flux was in the order of  $10^6 \text{ cm}^{-2} \text{ s}^{-1}$  with a beam spot uniformity of  $\pm 5\%$  within  $\sim 20 \text{ cm}$  diameter. The part of the thermal neutron flux represents less than  $1\%$  of the total integrated flux. Based on the NIEL of the InGaAs

material, the equivalent damage energy of the ANITA spectrum has been estimated to be around 2 MeV. Because the equivalent fluence at this energy in InGaAs and the associated damage dose used in this paper are the results of calculations, their values are subject to uncertainties.

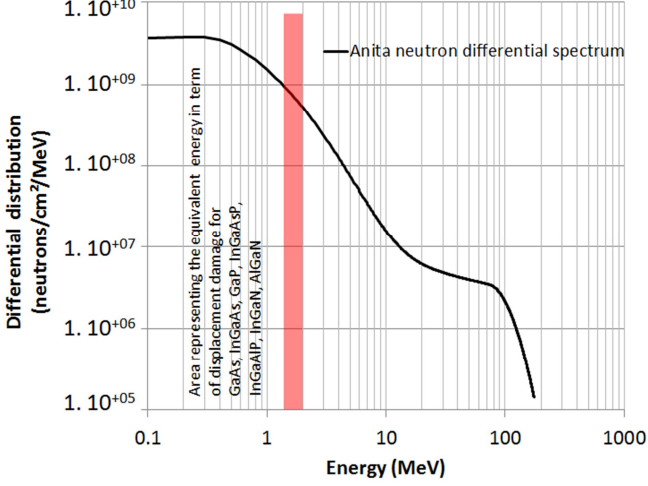


Fig. 1: Atmospheric-like neutrons spectrum provided by the ANITA facility. Depending on the tested material the equivalent damage energy is found to be in the order of 2 MeV.

Some Total Ionizing Dose (TID) tests have also been performed with the CNA  $^{60}\text{Co}$  facility (Centro Nacional de Aceleradores, Sevilla, Spain [34]), in order to check the sensitivity of the devices to the TID effect. The TABLE I summarizes the different irradiations performed on the devices.

### C. Test conditions

The photodiodes have been irradiated with two different bias conditions. Some devices have been shorted and the others have been irradiated with a reverse bias. This is the same bias conditions as those applied during the dark current measurements:  $-10\text{ V}$  for the C30618 (Excelitas) and  $-5\text{ V}$  for both SNAKE (Lynred) and FCIQ1000 (OSI). These biases correspond to a large depletion regime dominated by the generation current. The irradiations have been performed at ambient temperature ( $\sim 20^\circ\text{C}$ ). One device is irradiated per bias and energy. All the devices are irradiated de-lidded. One non-irradiated sample was measured as a reference at each step. The electrical measurements have been performed in a box with a controlled temperature close to  $24^\circ\text{C}$ . Both the Excelitas and OSI devices are placed in a well sized footprint of a thermally regulated copper plate inside the box. As a consequence, the temperature during the measurements is well controlled. The SNAKE test vehicles are just put into the box. This leads to a larger uncertainty of the device temperature during the measurements and a worse reproducibility. For the considered gap of InGaAs, considering a SRH carrier generation with an activation energy close to the mid gap, an error of  $1^\circ\text{C}$  around  $24^\circ\text{C}$  corresponds to an error of 5% in the dark current (close to 10% for  $2^\circ\text{C}$ ).

As can be seen in TABLE I, the applied fluences correspond to quite high levels of irradiation compared to most of the

space applications. The goal is to have a significant dark current increase that ensures some relevant measurements. For protons and high energy electrons, the final fluence and displacement damage dose change from one irradiation to another, but the final ionizing dose is quite the same, close to 320 Gy(InGaAs). For low energy electrons and gamma irradiations, the final dose is higher. But we provide intermediate steps at 300 Gy(InGaAs) for electron irradiations and 450 Gy(InGaAs) for gamma irradiation so that a comparison of the degradation at the same ionizing dose is quite possible. In a global point of view, intermediate fluence steps with dark current measurements in between have been performed for the neutron spectrum, the 170 MeV protons, the gamma rays, the 0.5 MeV and the 1.5 MeV electrons irradiations. In these cases, we can check the linearity of the dark current increase with the fluence. In terms of displacement damage dose, the maximum level is obtained for the ANITA neutron spectrum ( $\sim 2.4 \cdot 10^{10}\text{ MeV/g}$ ). The measurements have been performed within one hour after the end of the irradiation, this time depending on the access time to the irradiated samples (vacuum, activation). The dark current was measured two months after the irradiation in order to check the importance of the annealing processes.

TABLE I: THE DDD LEVELS APPLIED ON THE PHOTODIODES FOR ALL THE IRRADIATIONS.

Particle type	Energy (MeV)	Fluence (p./cm <sup>2</sup> )	TID level (Gy(InGaAs))	DDD level (MeV/g)
Neutrons (ANITA)	Spectrum	$3 \cdot 10^{11}$	NA	$6.9 \cdot 10^8$
		$3 \cdot 10^{12}$		$6.8 \cdot 10^9$
		$10^{13}$		$2.4 \cdot 10^{10}$
Protons (PAULA)	60	$3 \cdot 10^{11}$	320	$1.1 \cdot 10^9$
	100	$4.3 \cdot 10^{11}$	320	$1.5 \cdot 10^9$
	170	$3 \cdot 10^{11}$	152	$8.7 \cdot 10^8$
		$5 \cdot 10^{11}$	254	$1.4 \cdot 10^9$
		$6.3 \cdot 10^{11}$	320	$1.8 \cdot 10^9$
Electrons (ONERA)	0.5	$10^{12}$	200	$6.7 \cdot 10^6$
		$1.5 \cdot 10^{12}$	300	$1.0 \cdot 10^7$
		$2.5 \cdot 10^{12}$	500	$1.7 \cdot 10^7$
	1.5	$5 \cdot 10^{11}$	100	$1.5 \cdot 10^7$
		$10^{12}$	200	$2.9 \cdot 10^7$
		$1.5 \cdot 10^{12}$	300	$4.3 \cdot 10^7$
		$2 \cdot 10^{12}$	400	$5.8 \cdot 10^7$
Electrons (RADEF)	6	$1.18 \cdot 10^{12}$	325	$7.1 \cdot 10^7$
	12	$9.22 \cdot 10^{11}$	333	$7.1 \cdot 10^7$
	20	$7.16 \cdot 10^{11}$	339	$6.4 \cdot 10^7$
$^{60}\text{Co}$ (CNA)	1.25	up to $\sim 4.5 \cdot 10^{14}$ (*)	100	up to $\sim 4 \cdot 10^7$ (*)
			450	
			1050	
			2720	
			5240	

(\*) value estimated using the GaAs NIEL instead of the InGaAs one.

TABLE II: LIST OF THE IRRADIATIONS PER DEVICE TYPE.

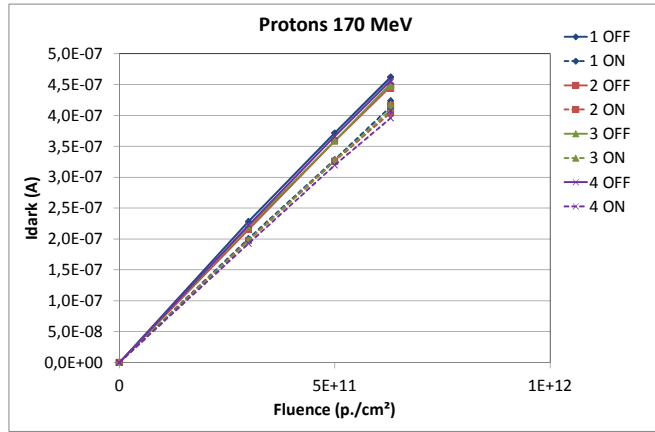
Particle	E (MeV)	SNAKE		OSI		Excelitas	
		OFF	ON	OFF	ON	OFF	ON
$n^\circ$	Spectrum	X	X	X	X	X	X
P+	60	X	X	X	X	X	X
	100			X	X	X	X
	170	X	X	X	X	X	X
e-	0.5	X		X	X	X	X
	1.5	X		X	X	X	X
	6	X		X		X	
	12	X					
	20	X		X		X	
$^{60}\text{Co}$	1.25	X	X	X	X	X	X

### III. EXPERIMENTAL RESULTS

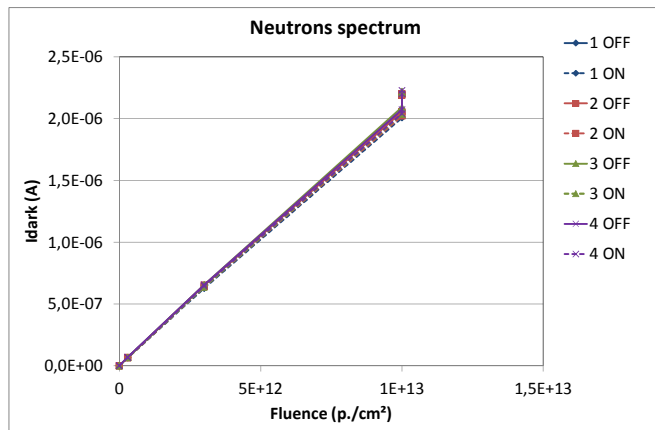
#### A. Dark current increase with fluence or ionizing dose

The Fig. 2 shows an example of the photodiode response with three different irradiation conditions: the 170 MeV protons, the ANITA neutron spectrum and the gamma. These three irradiations are selected because several fluences or dose levels are available. We can see that the dark current increase is linear with the fluence or the TID. This trend is true for the three types of photodiodes. This linear dependence will allow the extraction of a damage factor as described in the section IV.

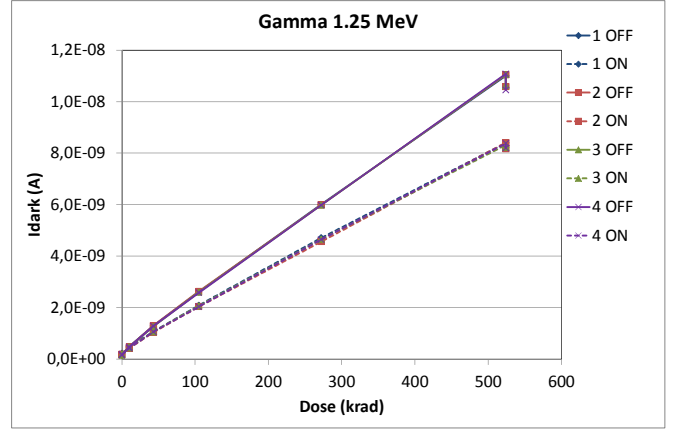
The final TID level for gamma irradiations (5240 Gy(InGaAs)) is much higher than the TID reached after the proton and electron irradiations (close to 320 Gy(InGaAs) for protons and up to 500 Gy(InGaAs) for electrons). The dark current increase is much lower for 500 Gy(InGaAs) gamma irradiation than for the other irradiations, except for 0.5 MeV electron where the degradation are similar. The conclusion is that, for 1.5 MeV or higher electrons energies, protons and neutron irradiations, the dark current degradation is dominated by displacement damage effects rather than TID effects.



(a)



(b)



(c)

Fig. 2: Dark current of the photodiodes FCIQ1000 (OSI) irradiated with (a) 170 MeV protons, (b) ANITA neutron spectrum and (c) gamma rays. Each figure detail the response of the four photodiodes of the device, irradiated biased or unbiased. The caption indicates the photodiode number and the bias condition during irradiation. The responses are linear as a function of the DDD or the TID.

The comparison between the 0.5 MeV electrons and the gamma irradiation must be detailed. We look at the cases of the OSI and Excelitas devices, where all the irradiated samples are the same for these two types of irradiations. The TABLE III gives the dark current increase of the devices after 0.5 MeV 500 Gy(InGaAs) (final step) and the gamma 430 Gy(InGaAs) irradiation. The latter is the closer intermediate irradiation step from the former. The TABLE III compares the absolute values and variations for the biased and unbiased devices. We can see that the degradation levels are very similar, especially after the two month annealing of the samples irradiated with 0.5 MeV electrons. We should note that the dose rate between gamma and electrons are very different (higher for electron) and that the yields of the two particles are slightly different. Nevertheless, we conclude that the TID effects are not negligible for 0.5 MeV electron irradiation, and may be the dominant contribution of the dark current increase. This remark will be used when comparing the damage factors with the NIEL in the section IV.

TABLE III: COMPARISON OF THE 430 Gy(INGAAS) GAMMA AND 500 Gy(INGAAS) 0.5 MeV ELECTRON IRRADIATIONS FOR THE OSI AND EXCELITAS PHOTODIODES DARK CURRENT.

Device	Gamma 430 Gy	0.5 MeV e- 500 Gy before annealing		0.5 MeV e- 500 Gy after annealing	
	$\Delta I$ (nA)	$\Delta I$ (nA)	Comp. $\gamma$	$\Delta I$ (nA)	Comp. $\gamma$
Excelitas OFF	1.58	2.28	30.7%	1.52	-4.1%
Excelitas ON	1.17	1.73	32.4%	1.27	7.8%
OSI OFF (*)	1.13	1.60	29.7%	1.06	-6.8%
OSI ON (*)	0.86	1.28	32.7%	0.96	9.8%

(\*) Mean value over the 4 samples of each device.

#### B. Bias effect

The bias effect is only observable when both ON and OFF irradiations are made for a given particle type and energy, i.e. for neutron, proton, and gamma irradiations for the three

device types, and for low energy electron irradiations for the OSI and Excelitas photodiodes (0.5 and 1.5 MeV), see TABLE II. The comparison is given in TABLE IV. For the proton and neutron irradiations, the difference is small and could be within the uncertainty of the measurements and temperature control. The difference is more sensible after gamma and low energy electron irradiation where the difference reached up to 25%. The general trend is a lower degradation of the biased devices during gamma irradiations.

TABLE IV: COMPARISON OF THE EFFECT OF THE BIAS CONDITIONS BEFORE ANNEALING.

Particle	E (MeV)	OSI(*)			Excelitas		
		$\Delta I$ (nA)		% OFF/ON	$\Delta I$ (nA)		% OFF/ON
		OFF	ON		OFF	ON	
n <sup>o</sup>	Spectrum	2070	2030	2%	2460	2340	5%
P+	60	202	213	-6%	233	218	6%
	100	289	307	-6%	301	277	8%
	170	454	406	11%	476	419	12%
e-	0.5	1.6	1.3	20%	2.3	1.7	26%
	1.5	10.6	10	5%	15.5	12.5	18%
<sup>60</sup> Co	1.25	10.9	8.2	25%	14.6	10.7	27%

(\*) Mean value over the 4 samples of each device.

### C. Annealing effect

The recovery processes at room temperature have been shown to be negligible even two months after the irradiations. This is also shown on the Fig. 2 (two points at the maximum fluence or ionizing dose). The detail of the annealing percentage is given in TABLE V. Most of the time, the annealing is close to 5% of the final dark current level just after irradiation for the OSI and Excelitas devices. Higher values of annealing are observed for the low energies electron irradiation. In this case, because the dark current increase is the lowest compared to the other irradiations, this behavior maybe both an effect of the ionizing degradation. The annealing of the SNAKE samples is close to 10%, within the uncertainty of the device temperature. The results presented in the rest of the paper correspond to the measurements two months after the irradiations.

TABLE V: EFFECT OF TWO MONTHS ANNEALING AT ROOM TEMPERATURE.

Particle	E (MeV)	SNAKE		OSI		Excelitas	
		OFF	ON	OFF	ON	OFF	ON
n <sup>o</sup>	Spectrum	1.6%	0.6%	-6.0%	-9.3%	-3.1%	
P+	60	11.5%	8.6%	-2.5%	-6.5%	0.9%	-4.1%
	100			1.9%	-1.5%	0%	-4.0%
	170	12.4%	9.6%	0.5%	-2.6%	-1.5%	-4.6%
e-	0.5	18.3%		27.4%	17.4%	33.4%	26.7%
	1.5	10.8%		19.5%	15.5%	18.7%	15.0%
	6	6.2%		6.0%		5.5%	
	12	-1.1%					
	20	-3.9%		3.8%		2.9%	
<sup>60</sup> Co	1.25	-2.4%	0.3%	4.5%	1.9%	2.2%	0.6%

### D. Effect of the photodiode dimension

In this paragraph, we specifically look at the relative degradation of the SNAKE photodiodes with respect to their surface. Indeed, all the photodiodes on the test vehicles are made in the same technology, which means that the vertical dimensions of the different photodiodes are the same. The

main difference from one diode to another is the topology (circular or square), the surface and the neighborhood (for the sub-arrays of pixels). So, if the dark current increase is due to defects in the volume of the semiconductor, it should be proportional to the surface of the different elements.

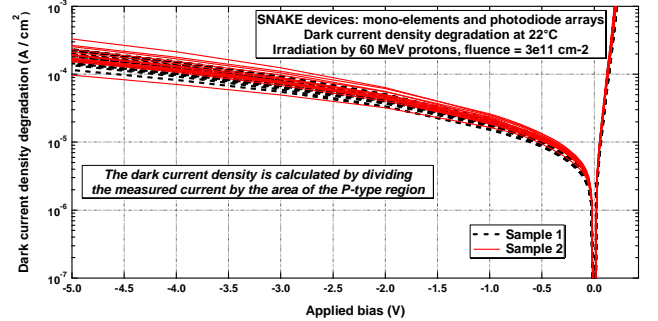


Fig. 3: I(V) curves of the different photodiode patterns. The current is normalized by the surface of the diodes (i.e. the diffused P-type area). Measurements at 22°C.

The comparison with the OSI and Excelitas devices is not possible because we do not have any information on the device structure, except the active surface. As a consequence, any differences in the doping concentrations, vertical dimensions... will induce a different active volume.

I(V) curves of all the patterns of the two test vehicles irradiated with 60 MeV protons (biased and unbiased) were measured several months after irradiation. The two test vehicles, labelled "Sample 1" and "Sample 2", come from two different InGaAs wafers. The Fig. 3 shows the normalized dark current degradation: the dark current after irradiation, much larger than the dark current before irradiation (see Fig. 2), is divided by the diode surface, defined by the area of the P-type region. The figure presents the curves of both the biased and unbiased test vehicles during irradiation. All the normalized curves follow the same trend within a factor of two. This confirms that the increase of the dark current is due to defects in the volume of the photodiodes. Note that the measurements of the dark current presented in the previous paragraphs on the SNAKE test vehicles were made at -5 V.

## IV. DARK CURRENT DAMAGE FACTOR

### A. Definition and evaluation

The damage factor is commonly used to compare the degradation of the devices for different particle types and energies due to displacement damage effects [6]-[8][16][18][19][23]. In our case, the damage factor is calculated by dividing the dark current increase by the fluence  $\Phi$ .

$$K_{I_{dark}} = \frac{I_{dark}(\Phi) - I_{dark}(0)}{\Phi} = \frac{\Delta I_{dark}(\Phi)}{\Phi} \quad (1)$$

with  $I_{dark}(\Phi)$  the dark current at the fluence  $\Phi$  and  $I_{dark}(0)$  the initial dark current.

We should note that the dark current increase is due to both ionizing ( $\Delta I_{dark,i}$ ) and non-ionizing ( $\Delta I_{dark,ni}$ ) effects:

$$\Delta I_{dark}(\Phi) = \Delta I_{dark,i}(\Phi) + \Delta I_{dark,ni}(\Phi) \quad (2)$$

As a consequence, the measured damage factor is the sum of a ionizing and a non-ionizing contribution:

$$K_{I_{dark}} = K_{I_{dark,i}} + K_{I_{dark,ni}} \quad (3)$$

with  $i$  and  $ni$  referring to ionizing and non-ionizing effects respectively. The concept here is possible because both the ionizing and non-ionizing dark current increase are proportional to the TID and the fluence respectively.

In our case, we intend to compare the non-ionizing damage factor  $K_{I_{dark,ni}}$ , related to the effect of the displacement damages, with the NIEL. The presence of any ionizing contribution in the measurement of  $\Delta I_{dark}(\Phi)$  introduces an error in this estimation. Nevertheless, we saw that, for all the irradiations but 0.5 MeV electrons, the dark current increase was dominated by the displacement damages. In these cases,  $K_{I_{dark,i}} \ll K_{I_{dark,ni}}$  and  $K_{I_{dark}} \simeq K_{I_{dark,ni}}$ . For the 0.5 MeV electrons,  $K_{I_{dark,i}}$  is not negligible anymore. Because it is difficult to determine the ionizing contribution in the dark current increase, we can only remark that  $K_{I_{dark,ni}} < K_{I_{dark}}$ . As a conclusion, the evaluation of  $K_{I_{dark,ni}}$  is not distorted by the ionizing effects for all the irradiations, except for the 0.5 MeV electron irradiation where it is overestimated. This will be reminded in the following paragraph.

The majority of the thermal annealing processes, if any, are believed to have taken place in the first few days following irradiation. In order to take them into account and to get the “final state” of the displacement damage, the damage factor is evaluated with the measurements made two months after irradiation. Anyway, the previous section showed that the annealing is small for our devices.

In the evaluation of the damage factor, we divide the dark current by the surface of the photodiode. For the OSI and Excelitas devices, we use the optimal surface of the devices (350  $\mu\text{m}$  diameter,  $9.62 \cdot 10^{-4} \text{ cm}^2$  for Excelitas, 4 quadrants of one 1000  $\mu\text{m}$  diameter,  $7.85 \cdot 10^{-3} \text{ cm}^2$  each). For the SNAKE test vehicle, we divide the current by the diffusion surface evaluated by LYNRED, smaller than the pitch of the photodiode. This point will be discussed in the following paragraph.

Finally, we focus in this paper on the comparison of the damage factors from one energy or particle type to another. They are compared to the relative variation of the NIEL of the InGaAs material. For these reasons, the damage factors are normalized to the NIEL at a given particle type and energy. As a consequence, we evaluate the relative damage factor  $rel K_{I_{dark}}(Part., E)$  for a given particle type  $Part.$  at the energy  $E$  with the following formula:

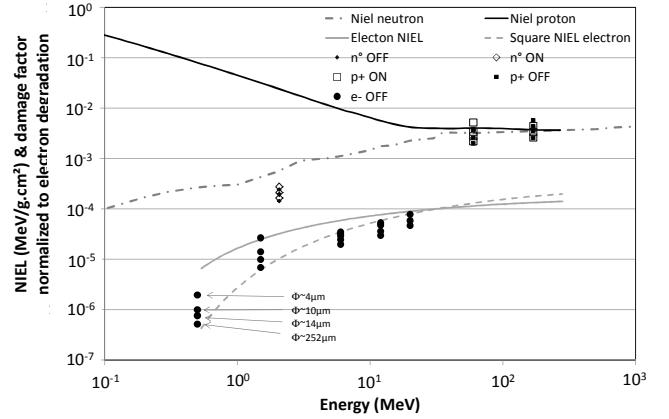
$$rel K_{I_{dark}}(Part., E) = \frac{K_{I_{dark}}(Part., E)}{K_{I_{dark}}(Part_0., E_0)} NIEL(Part_0., E_0) \quad (4)$$

where  $(Part., E)$  is a couple of particle type and energy, the subscript 0 is for the couple of reference chosen for the normalization. In the following paragraphs, the data are normalized to the neutron results because no ionizing effects are expected after such irradiation. Indeed,  $K_{I_{dark}}(Part_0., E_0)$  is the mean value of the damage factor (over the different bias

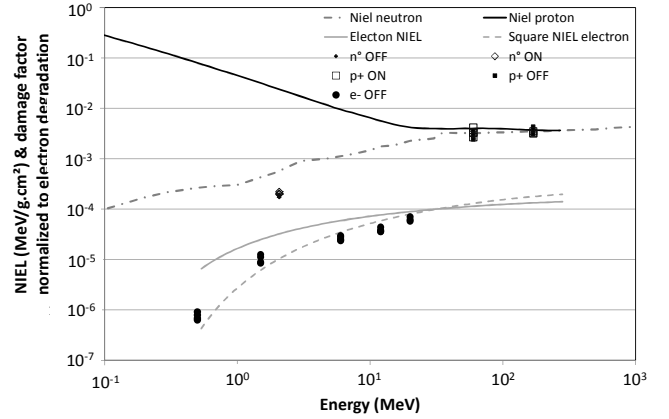
and topologies within a device type) for the neutron irradiation and  $NIEL(Part_0., E_0)$  is equal to the NIEL of the InGaAs for 2.07 MeV neutrons ( $5.71 \cdot 10^{-4} \text{ MeVcm}^2/\text{g}$ ). Nevertheless, because the equivalent fluence for neutron irradiations is subject to uncertainties (as presented in II.B), we will see that the result of the calculation of the damage factor needs to be corrected by a factor of two generally if we intend to fit the data to the NIEL of other particles. This will be detailed in the presentation of the results.

### B. SNAKE relative damage factor

We first intend to clarify the right evaluation of the damage factor for the SNAKE test vehicles. Indeed, the particularity of these samples is that different topologies are available and we want to check the consistency of the different results.



(a)



(b)

Fig. 4: Comparison between the dark current increase experimental damage factors for the SNAKE test vehicles and the NIEL of InGaAs. (a) using the diffusion surface evaluated by LYNRED and (b) by correcting the diameter by 2.5  $\mu\text{m}$ .

The Fig. 4 (a) presents the damage factor of all the available data. The experimental relative damage factors normalized to the neutron irradiations are corrected by a factor of two in order to scale with proton NIEL. We see a dispersion in the data. In particular, the result for low electron energies is spread over a factor of five. We must note that, in contrary to

the OSI and Excelitas samples that have both large dimensions, some SNAKE samples have diffusion diameters down to 4  $\mu\text{m}$ . Any error in the evaluation of the diffusion diameter could lead to an error in the damage factor. Such a difference could occur if the theoretical and effective diameters differ due for example to the manufacturing processes.

In Fig. 4 (b), we introduce an offset in the diffusion diameter close to 2.5  $\mu\text{m}$ , corresponding to an increase of the diffusion diameter. This correction was suggested by the manufacturer. Indeed, this small value has a great impact on the small dimensions and the effect is clearly a homogenization of the results. In the following paragraphs, we will keep this hypothesis for the analysis of the comparison of the damage factors with the NIEL. Once again, for the large photodiode dimensions (SNAKE, OSI and Excelitas), the diffusion area is close to the optimal diameter of the topology and these two surfaces are almost the same.

### C. Proton relative damage factor for all the device types

In the Fig. 5, we compare the damage factors with the NIEL for proton irradiations with the same normalization factor than in Fig. 4 (i.e. neutron and a factor of two for all the devices). We see that, for the three device types, the damage factor follows the total NIEL. This is a difference compared to other publications that reported a damage factor decreasing with the proton energy above some tens of MeV, sometimes following the curve of the Coulombic part of the NIEL.

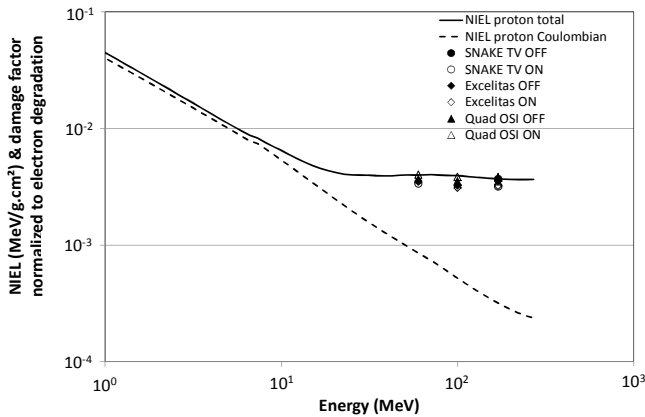


Fig. 5: Comparison between the dark current increase experimental damage factors and the NIEL of InGaAs for protons. The SNAKE data correspond to the mean value over the different sizes of photodiodes.

### D. Electron relative damage factor for all the device types

In Fig. 6, we present the shape of the damage factors compared to the electron NIEL. We should note that, for such a comparison, we used different scale factors for the OSI and Excelitas devices than for the SNAKE. This will be clearly visible in the following paragraph where we present all the damage factors together. The consequence here is that we propose a comparison of the shape of the variation of the damage factors with the NIEL.

The general trend is that the variation of the damage factors is bigger than the electron NIEL. Indeed, the variation of the damage factors between 0.5 MeV and 20 MeV is close to a

factor of one hundred, whereas the variation of the NIEL is close to a factor of ten. This behaviour is closer to the variation of the square of the NIEL, which is also represented on the figure. Such behaviour has been observed for silicon devices [6]. An explanation was given in [36], related to a worse calculation of the low NIEL values.

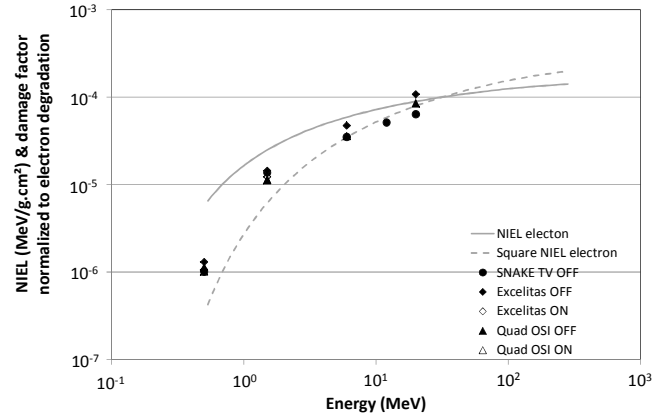


Fig. 6: Comparison between the dark current increase experimental damage factors and the NIEL of InGaAs for electrons. The SNAKE data correspond to the mean value over the different sizes of photodiodes.

### E. Relative damage factors for all devices and particle types

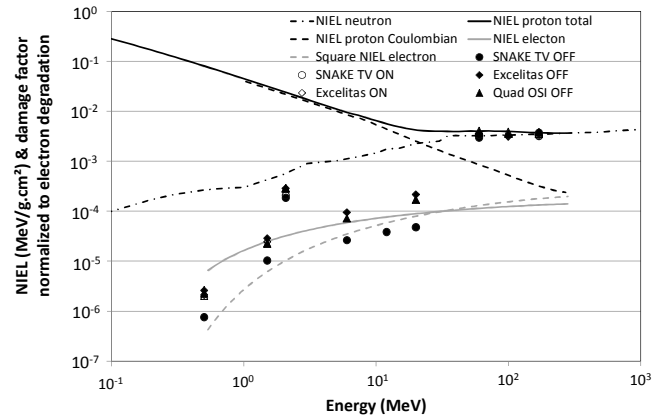


Fig. 7: Comparison between the dark current increase experimental damage factors and the NIEL of InGaAs for neutrons, protons and electrons. The SNAKE data correspond to the mean value over the different sizes of photodiodes.

Finally, the Fig. 7 compares the damage factors all together. The normalization factor is the same for the three device types, i.e. a factor of two applied on the neutron damage factor. In this case, we see that 1) with this choice, the proton data fit with the NIEL, 2) the neutron data are lower than the neutron NIEL and 3) the electron data are spread around the electron NIEL. We could have chosen to normalize the data for the best fit with electron or neutron results. This would have shifted the data up or down. But at this stage, it is difficult to conclude on the best way to normalize the data. Anyway, because of the complex spectrum of the neutron irradiation and its uncertainties in the evaluation of the equivalent energy and fluence, the difference between the neutron NIEL and the damage factors should not be

considered as abnormal (factor two). But one must retain that the gap between the proton and electron damage factors is not the same for the OSI and Excelitas devices on one side, and the SNAKE test vehicles on the other side. Fig. 7 shows that a factor close to four between all these data remains after normalization.

## V. CONCLUSION

This work shows some irradiation data of the dark current increase in different InGaAs photodiodes. The current increases linearly with the fluence or the TID. The degradation of the different topologies of photodiodes is consistent with a degradation in the volume of the device. The experimental damage factors are compared with the NIEL for InGaAs material. The results show some differences in the ratio between proton and electron results from device type to device type. The damage factors follow the total NIEL for high energy protons and the electron NIEL overestimates the low energy electron damage factors.

## REFERENCES

- [1] S. R. Messenger, E. A. Burke, G. P. Summers, M. A. Xapsos, R. J. Walters, E. M. Jackson, and B. D. Weaver, "Non ionizing energy loss (NIEL) for heavy ions," *IEEE Trans. Nucl. Sci.*, vol. 46, no. 6, pp. 1595–1602, Dec. 1999.
- [2] A. Akkerman, J. Barak, M. B. Chadwick, J. Levinson, M. Murat, and Y. Lifshitz, "Updated NIEL calculations for estimating the damage induced by particles and gamma-rays in Si and GaAs," *Rad. Phys. and Chem.*, vol. 62, pp. 301–310, 2001.
- [3] I. Jun, W. Kim, and R. Evans, "Electron nonionizing energy loss for device applications," *IEEE Trans. Nucl. Sci.*, vol. 56, no. 6, pp. 3229–3235, Dec. 2009.
- [4] C. Inguibert, and R. Gigante, "NEMO: A code to compute NIEL of protons, neutrons, electrons, and heavy ions," *IEEE Trans. Nucl. Sci.*, vol. 53, no. 4, pp. 1967–1972, Aug. 2006.
- [5] M. J. Boschini, C. Consolandi, M. Gervasi, S. Giani, D. Grandi, V. Ivanchenko, P. Nieminem, S. PenBotti, P. G. Rancoita, M. Tacconi, E. ESA, and A. G. Noordwijk, "Nuclear and non-ionizing energy-loss for Coulomb scattered particle from low energy up to relativistic regime in space radiation environment," in *Proc. the 12th ICATPP Conference on Astroparticle, Particle, Space Physics and Detectors for Physics Applications*, Como, Italy, pp. 9–23, Oct. 2010.
- [6] J. R. Srour, "Review of displacement damage effects in silicon devices," *IEEE Trans. Nucl. Sci.*, vol. 50, no. 3, pp. 653–670, Jun. 2003.
- [7] J. R. Srour, J. W. Palko "A framework for understanding displacement damage mechanisms in irradiated silicon devices," *IEEE Trans. Nucl. Sci.*, vol. NS-53, no. 6, pp. 3610–3620 December 2006
- [8] G. P. Summers, E. A. Burke, C. Dale, E. A. Wolicki, P. W. Marshall, M. A. Gehlhausen, "Correlation of Particle-Induced Displacement Damage in Silicon," *IEEE Trans. Nucl. Sci.*, vol. 34, no. 6, pp. 1133–1139, Dec. 1987.
- [9] S. R. Messenger G. P. Summers, E. A. Burke, R. J. Walters, and M. A. Xapsos, "Modeling solar cell degradation in space: A comparison of the NRL displacement damage dose and JPL equivalent fluence approaches," *Progress in Photovoltaics: Research and Applications*, vol. 9, pp. 103–121, 2001.
- [10] K. Thommen, "Recovery of low temperature electron irradiation-induced damage in n-type GaAs," *Radiation effects*, vol. 2, no. 3, pp. 201–210, 1970.
- [11] A. H. Kalma, R. A. Berger, C. J. Fischer, and B. A. Green, "Energy and temperature dependence of electron irradiation damage in GaAs," *IEEE Trans. Nucl. Sci.*, vol. 22, no. 6, pp. 2277–2282, Dec. 1975.
- [12] D. Pons, P. M. Mooney, and J. C. Bourgoin, "Energy-dependence of deep level introduction in electron-irradiated GaAs," *J. Applied Phys.*, vol. 51, no. 6, pp. 2038–2042, Apr. 1980.
- [13] M. Yamaguchi, C. Amano, "<sup>60</sup>Co  $\gamma$ -ray and electron irradiation damage of GaAs single crystals and solar cells," *J. Applied Phys.*, vol. 54, no. 9, pp. 5021–5029, Sep. 1983.
- [14] A. Meulenber, C. M. Dozier, W. T. Anderson, S. D. Mittleman, M. H. Zuglich, and C. E. Caefer, "Dosimetry and total dose radiation testing of GaAs devices," *IEEE Trans. Nucl. Sci.*, vol. 34, no. 6, pp. 1745–1750, Dec. 1987.
- [15] M. A. Xapsos, G. P. Summers, C. C. Blatchley, C. W. Colerico, E. A. Burke, S. R. Messenger and P. Shapiro, "Co60 Gamma Ray and Electron Displacement Damage Studies of Semiconductors," *IEEE Trans. Nucl. Sci.*, vol. 41, no. 6, pp. 1945–1949, Dec. 1994.
- [16] G. P. Summers, E. A. Burke, P. Shapiro, S. Messenger, and R. J. Walters, "Damage correlations in semiconductors exposed to gamma, electron and proton radiations," *IEEE Trans. Nucl. Sci.*, vol. 40, no. 6, pp. 1372–1379, Dec. 1993.
- [17] G. P. Summers, E. A. Burke, and M. A. Xapsos, "Displacement damage analogs to ionizing radiation effects," *Rad. Meas.*, vol. 24, no. 1, pp. 1–8, 1995.
- [18] J. H. Warner, S. R. Messenger, R. J. Walters, G. P. Summers, J. R. Lorentzen, D. M. Wilt, M. A. Smith, "Correlation of electron radiation induced damage in GaAs solar cells," *IEEE Trans. Nucl. Sci.*, vol. 53, no. 4, pp. 1988–1994, Aug. 2006.
- [19] J. H. Warner, S. R. Messenger, R. J. Walters, G. P. Summers, "A comparison between p-n and n-p GaAs displacement damage coefficients following proton irradiation," *33rd IEEE Photovoltaic Specialists Conference*, pp. 1-5, 2008.
- [20] P. Arnolda, C. Inguibert, T. Nuns, C. Boatella-Polo, "NIEL scaling: comparison with measured defect introduction rate in silicon," *IEEE Trans. Nucl. Sci.*, vol. 58, no. 3, pp. 756–763, Jun. 2011.
- [21] E. EL Allam, C. Inguibert, T. Nuns, A. Meulenber, A. Jorio, I. Zorkani, "Gamma and Electron NIEL Dependence of Irradiated GaAs," *IEEE Trans. Nucl. Sci.*, vol. 64, no. 3, pp. 991–998, Mar. 2017.
- [22] G. P. Summers, E. A. Burke, M. A. Xapsos, C. Dale, P. W. Marshall, E. L. Petersen, "Displacement damage in GaAs structures," *IEEE Trans. Nucl. Sci.*, vol. 35, no. 6, pp. 1221–1226, Dec. 1988.
- [23] S. R. Messenger, R. J. Walters, E. Burke, G. P. Summers, and M. A. Xapsos, "NIEL and damage correlations for high-energy protons in gallium arsenide devices," *IEEE Trans. Nucl. Sci.*, vol. 48, no. 6, pp. 2121–2126, Dec. 2001.
- [24] A. M. Ougouag, J.G. Williams, M. B. Danjaji, J. L. Yang, J. L. Meason, "Differential displacement kerma cross sections for neutron interactions in Si and GaAs," *IEEE Trans. Nucl. Sci.*, vol. 37, no. 6, Part II, pp. 2219–2228, Dec. 1990.
- [25] O. Gilard, L. S. How, A. Delbergue, C. Inguibert, T. Nuns, J. Barbero, J. Moreno, L. Bouet, S. Mariojouis, M. Boutillier, "Damage Factor for Radiation-Induced Dark Current in InGaAs Photodiodes," *IEEE Trans. Nucl. Sci.*, vol. 65, no. 3, Part II, pp. 884–895, Mar. 2018.
- [26] GEODUR: Chambre d'irradiation électrons multi applications (matériaux, composants, charge interne des isolants. [Online]. Available: <http://www.onera.fr/fr/desp/geodur> Accessed July 27, 2017.
- [27] RADEF: Jyväskylä Yliopisto, University of Jyväskylä. [Online]. Available: <https://www.jyu.fi/fysiikka/en/research/accelerator/radef>. Accessed July 27, 2017.
- [28] The ANITA neutron beam facility [Online]. Available: [http://www.tsl.uu.se/irradiation-facilities-tsl/ANITA\\_neutron\\_beam\\_facility/](http://www.tsl.uu.se/irradiation-facilities-tsl/ANITA_neutron_beam_facility/) Accessed July 27, 2017.
- [29] The European Defence Agency [Online]. Available: <https://www.eda.europa.eu/> Accessed July 27, 2019.
- [30] OMERE: Outil de Modélisation de l'Environnement Radiatif Externe, version 4.2. [Online]. Available: <http://www.trad.fr/OMERE-14.html> Accessed July 27, 2017.
- [31] LYNRED: Lynred [Online]. Available: <https://www.lynred.com> Accessed September 10, 2019; notice that Sofradir became Lynred in 2019.
- [32] EXCELITAS: Excelitas technologies. [Online]. Available: <http://www.excelitas.com/Pages/Index.aspx> Accessed July 27, 2017.
- [33] OSI: OSI Optoelectronics. [Online]. Available: <http://www.osioptoelectronics.com/standard-products/silicon-photodiodes.aspx> Accessed July 27, 2017.
- [34] CAN: Centro Nacional de Aceleradores [Online]. Available: <http://www.centro.us.es/cna/index.php/en/facilities/co-60-irradiator> Accessed April 10, 2019.
- [35] P. V Dressendorfer, "Ionizing radiation effects in MOS devices and circuits," Wiley Interscience publication, 1989.
- [36] C. Inguibert, P. Arnolda, T. Nuns, G. Rolland, "Effective NIEL in Silicon: Calculation using molecular dynamic results," *IEEE Trans. Nucl. Sci.*, vol. 57, no. 4, pp. 1915–1923, 2010.